

Resonant Field Enhancement of Epsilon Near Zero Berreman Modes in an Ultrathin AlN Film

Nikolai Christian Passler,^{*,†} Ilya Razdolski,[†] D. Scott Katzer,[‡] David F. Storm,[‡]
Joshua D. Caldwell,^{‡,¶} Martin Wolf,[†] and Alexander Paarmann^{*,†}

[†]*Fritz-Haber-Institut der Max-Planck-Gesellschaft, Faradayweg 4-6, 14195 Berlin, Germany*

[‡]*US Naval Research Laboratory, 4555 Overlook Avenue SW, Washington DC 20375, USA*

[¶]*Vanderbilt Institute of Nanoscale Science and Engineering, 2201 West End Ave, PMB 350106, Nashville, TN 37235-0106, USA*

E-mail: passler@fhi-berlin.mpg.de; alexander.paarmann@fhi-berlin.mpg.de

Abstract

Enormous optical field enhancement was predicted to occur for the Berreman mode in ultrathin films in the vicinity of epsilon near zero (ENZ). Here, we report the first experimental proof of this prediction in the mid-infrared by probing the resonantly enhanced second harmonic generation (SHG) at the longitudinal optic phonon frequency from a deeply subwavelength-thin aluminum nitride (AlN) film. Employing a transfer matrix formalism, we show that the field enhancement is completely localized inside the AlN layer, revealing that the observed SHG signal of the Berreman mode is solely generated in the AlN film. Our results demonstrate that ENZ Berreman modes in intrinsically low-loss polar dielectric crystals constitute a promising platform for nonlinear nanophotonic applications.

Keywords

Berreman mode, epsilon near zero, infrared, nanophotonics, second harmonic generation, field enhancement

In nanophotonics, nonlinear optical phenomena are driven by the enhancement of local optical fields, which arises due to polaritonic resonances. These are traditionally observed

as plasmon polaritons in metallic nanostructures or rough metal surfaces. Such strongly enhanced fields enable a variety of nanoscale applications¹ such as all-optical switching,^{2,3} low-loss frequency conversion,^{4,5} and highly efficient sensing.^{6,7} In the infrared (IR), an alternative to plasmonic resonances in metals are phonon polaritons supported in polar crystals,⁸ as has been demonstrated in various seminal studies.⁹⁻¹² These phonon polaritons feature longer lifetimes than plasmon polaritons, leading to much larger quality factors and stronger field enhancements,¹³⁻¹⁵ and thus potentially enhanced efficiency of nonlinear optical effects.

One area in nanophotonics of distinct recent interest are investigations of polaritonic modes in plasmonic or polar dielectric subwavelength-thin films that emerge near zero permittivity. Over the past decades, the existence of such thin-film polaritonic modes has attracted broad attention.¹⁶⁻²⁴ Initially, radiation in a narrow spectral window at the plasma frequency of thin metal films was predicted¹⁶ and later observed.¹⁸⁻²⁰ Its origin was associated with a collective surface plasma mode with polarization normal to the surface plane of the film.¹⁸ At the same time, a similar effect was reported by Berreman in a thin polar dielectric film,¹⁷ where absorption occurs at the longitudinal optic (LO) phonon frequency.

These absorption features in thin films were

argued to originate in radiative virtual polaritonic modes,^{21–23} naturally occurring at frequencies where the real part of the dielectric function crosses zero. This condition is met at the plasma frequency in a metal, and at the LO frequency of a polar crystal film. While these lossy polariton modes disperse on the low momentum side of the light line, it was discovered that a complementary evanescent polariton mode close to the LO frequency of a polar dielectric is also supported outside the light cone.²² Just like the radiative modes, the evanescent polaritons naturally emerge in thin films at frequencies of vanishing dielectric function. Therefore, these modes offer an intriguing platform for exploiting the unique characteristics of waves propagating in so called epsilon near zero (ENZ) materials.^{25,26}

While most ENZ studies depend on carefully and intricately designed metamaterials,^{27–29} thin metal or polar dielectric films stand out for their structural simplicity. Previous studies have reported promising applications employing these ENZ polariton modes, such as optoelectronic devices for the ultrafast control of absorption and emissivity,^{30–32} directionally perfect absorption,^{33,34} or long-range plasmon polaritons for the development of nanophotonic integrated technologies.^{35,36}

However, these previous studies mostly focused on the linear optical response, whereas only few reports of the nonlinear conversion efficiency of ultrathin films exist. This efficiency has been proposed to be strongly enhanced at ENZ frequencies,³⁷ but experimental verification is limited to a few studies of indium tin oxide (ITO) thin layers^{38–40} excited at frequencies in the near infrared spectral range. The nonlinear optical response of thin films of other materials with phonon resonances in the mid-to far-IR, in particular III-V or III-nitride polar semiconductor compounds, however, has to the best of our knowledge not yet been studied.

In this work, we investigate the linear and nonlinear optical response of ultrathin ($\lambda/1000$) AlN films on a SiC substrate in the radiative regime, where λ represents the free-space wavelength at the ENZ condition. We report strong SHG at the AlN LO phonon

frequency arising from the Berreman mode in the ultrathin AlN film. The observed SHG yield provides experimental proof of the immense field enhancement inside the film and is attributed to the excitation of the Berreman resonance. Furthermore, we delineate several perspectives based on ENZ polaritons for the deployment of low-loss nonlinear nanophotonic applications.

A mode in a medium is defined as a solution of Maxwell’s equations in the absence of an external perturbation. In a three-layer system, the dispersion of a polaritonic mode can be calculated by numerical evaluation of the following formula:^{20,24,41}

$$1 + \frac{\varepsilon_1 k_{z3}}{\varepsilon_3 k_{z1}} = i \tan(k_{z2}d) \left(\frac{\varepsilon_2 k_{z3}}{\varepsilon_3 k_{z2}} + \frac{\varepsilon_1 k_{z2}}{\varepsilon_2 k_{z1}} \right), \quad (1)$$

where ε is the dielectric function, d is the film thickness of layer 2, $k_{zi} = \sqrt{\frac{\omega^2}{c^2} \varepsilon_i - k_x^2}$ is the out-of-plane momentum, k_x is the in-plane momentum conserved in all layers, and the subscripts $i = 1, 2, 3$ refer to the three layered media. Note that all solutions shown here are calculated assuming a complex frequency ω and solved for a real wavevector k_x .

By solving Eq. 1 for an air/AlN/air system with varying thickness d_{AlN} of the AlN layer, the dispersion curves shown in Fig. 1a are obtained. On the right hand side of the light line, i.e. in the region of evanescent surface-bound solutions, the symmetric (upper blue lines) and antisymmetric (lower blue lines) thin-film polaritons emerge. Spectrally, these modes are bound inside the AlN reststrahlen region between the TO and LO frequencies ω_{TO}^{AlN} and ω_{LO}^{AlN} , respectively. For thick films ($d_{AlN} > 1 \mu\text{m}$), the two modes enclose the dispersion of a surface phonon polariton (SPhP) at the interface of a bulk AlN crystal (green line) and, for further increasing film thicknesses, eventually fall back onto this single green curve. On the other hand, for diminishing thicknesses, the two modes are pushed towards ω_{TO}^{AlN} and ω_{LO}^{AlN} . For $d_{AlN} = 20 \text{ nm}$ (solid line), the upper mode features a flat dispersion curve in the vicinity of ω_{LO}^{AlN} . At this frequency, the dielectric function

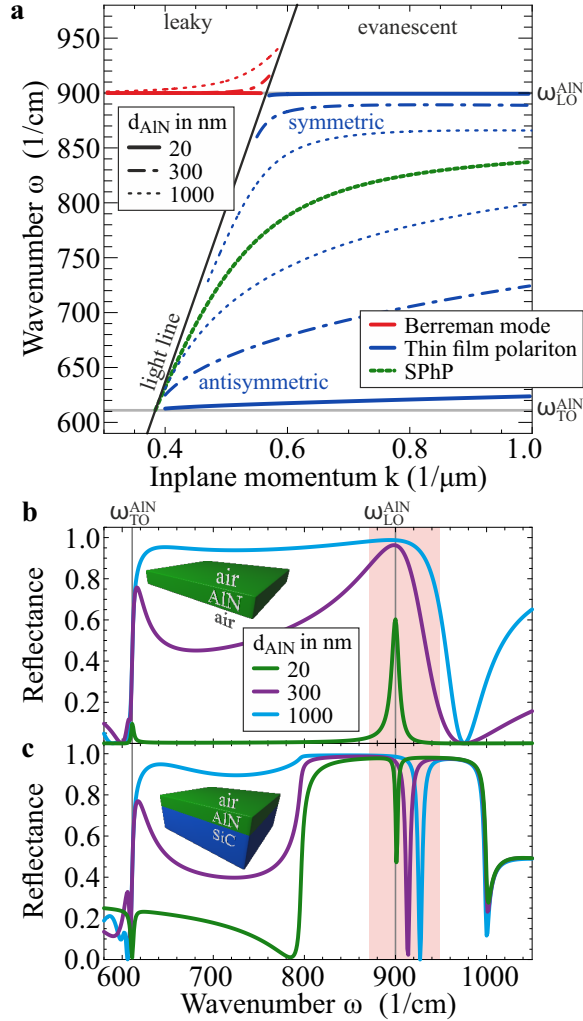


Figure 1: **Berreman mode in a freestanding AlN film and on a SiC substrate.** **a** Calculated dispersions of the Berreman mode and thin film polaritons in a freestanding AlN film, and that of a SPhP at the surface of a bulk AlN crystal. The Berreman mode is flat (red line) for ultrathin films ($d < \lambda/500$), while thicker films (dash dotted/dotted red lines) result in a dispersion bending upwards in the vicinity of the light line in vacuum (black line). Analogous to the symmetric thin film polariton (blue line, upper branch), the dispersion of the Berreman mode lies close to the LO frequency where the real part of the dielectric function exhibits a zero-crossing. **b** Calculated reflectance of a freestanding AlN thin film for three different film thicknesses d_{AlN} at an incidence angle of 85° . The peak at the LO frequency for the thinnest film corresponds to the Berreman mode (red shade), which transforms into the upper edge of the reststrahlen band for increasing film thicknesses. **c** The same calculation as in b is shown with a SiC substrate instead of air. Here, the Berreman mode appears as a deep dip inside the reststrahlen band of SiC.

approaches zero, and hence the upper mode is an ENZ thin-film polariton.

The Berreman mode (red lines) arises as a continuation on the left hand side of the light line, i.e. in the region of radiative solutions. Contrary to its evanescent counterpart, this leaky polariton mode undergoes a small upward bend close to the light line for larger film thicknesses. For $d_{AlN} = 20$ nm, however, the Berreman mode exhibits a flat dispersion at ω_{LO} just like the evanescent polariton, and therefore also exhibits ENZ character.

The feature at the LO frequency originally reported by Berreman¹⁷ is reproduced in the reflectance simulations shown in Fig. 1b. The Berreman mode can only be excited by radiation with a non-zero out-of-plane electric field component, and hence p -polarized light at oblique incidence is required to observe the absorption peak. In order to accentuate the Berreman absorption feature, the curves shown in Fig. 1b-c were calculated at an incidence angle of 85° , leading to a strongly pronounced peak at $\omega_{LO}^{AlN} = 900$ cm $^{-1}$ for $d_{AlN} = 20$ nm.

The transition from an ultrathin AlN film with $d_{AlN} = 20$ nm to a thicker one with $d_{AlN} = 1000$ nm, as demonstrated in Fig. 1b, is characterized by the buildup of the AlN reststrahlen band. Already for $d_{AlN} = 300$ nm, the Berreman absorption peak is strongly broadened and its frequency position is not clearly defined. This is different in Fig. 1c, where we show the same reflectance curves for an air/AlN/SiC structure, resembling the experimentally investigated sample. Interestingly, the Berreman absorption feature is inverted, appearing as an absorption dip inside the highly reflective reststrahlen band of the SiC substrate. In contrast to the freestanding film, a sharp and deep minimum is observed even for 1000 nm film thickness, indicating that the Berreman mode is still supported at the thick-film limit. This is corroborated by the frequency position of the feature, being in agreement with the dispersion curve in Fig. 1a.

In order to probe the field enhancement associated with the excitation of the Berreman mode, we employ SHG spectroscopy.⁴² The strongest field confinement occurs in ultrathin

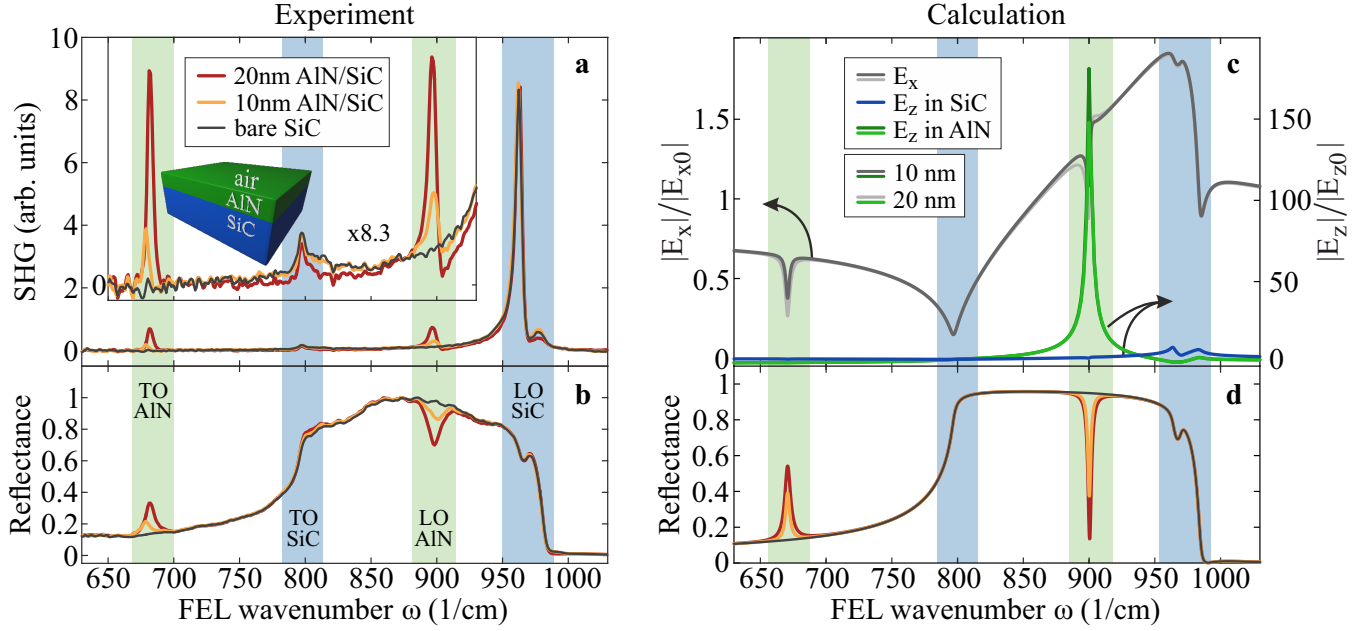


Figure 2: **Strongly enhanced SHG from a Berreman mode in AlN.** **a** and **b** show the experimental SHG and reflectance spectra, respectively, taken for three samples consisting of (i) a 20 nm, (ii) a 10 nm thin AlN film on a 4H-SiC substrate, and (iii) a bare 4H-SiC crystal. Compared to the reference sample (iii), the AlN thin films only differ at the TO and LO frequencies of AlN, exhibiting small features in the reflectance and a strong SHG signal (enlarged by a factor of 8.3 in the inset in **a**). The origin of the strong SHG yield is illustrated in **c**. While the in-plane E_x field enhancement is small at the AlN/SiC interface (grey lines, left y-axis), the out-of-plane E_z fields feature a gigantic enhancement of > 150 at the AlN LO frequency (green lines, right y-axis). On the SiC side of the AlN/SiC interface, the E_z fields are small (blue line), revealing that the field enhancement is strictly confined inside the nanometric AlN layer. **d** shows calculated reflectance curves of the investigated samples, being in excellent agreement with the experiment.

films leading to an enormous field enhancement of the Berreman mode, which is a prerequisite for the observation of a significant SHG signal. We therefore focus on two samples with ultrathin AlN films of thickness $d_{\text{AlN}} = 10$ nm and 20 nm. The AlN films were grown by RF-plasma assisted molecular beam epitaxy onto a 4H-SiC substrate, and therefore also feature a hexagonal crystal structure with the c -axis being perpendicular to the sample surface.

The reflectance and SHG spectroscopy measurements were performed in a non-collinear autocorrelator setup⁴² at 30° and 60° incidence angle employing a tunable, narrow-band, p -polarized mid-IR free electron laser (FEL)⁴³ as an excitation source. Beforehand, intrinsic higher harmonics of the FEL are blocked by two dichroic $7\ \mu\text{m}$ longpass filters. The reflectance is recorded at 60° by a pyroelectric detector,

whereas the two-pulse correlated SHG signal is generated at 45° between the reflected fundamental beams and is measured by a mercury-cadmium-telluride detector. We note that the non-collinear excitation scheme is only applicable for ultrathin films where the shift of the Berreman resonance frequency with incidence angle is negligible (see Fig. 1a), whereas for thicker films, a collinear setup would be necessary.⁴⁴

The experimental SHG and reflectance spectra are plotted in Figs. 2a and b, respectively. There, the yellow and red lines indicate the data for the 10 and 20 nm thick AlN films, respectively. Additionally, we show spectra for a bare SiC sample (black lines). As has been demonstrated previously,^{42,45} the bulk SiC substrate produces SHG peaks at its TO and LO frequencies (blue shades), leading to the same

response in all three samples in these regions ($\omega \sim 800 \text{ cm}^{-1}$ and $\omega \sim 970 \text{ cm}^{-1}$). In fact, the only deviations from the bulk reflectance and SHG spectra are seen at the AlN TO and LO frequencies (green shades), where we observe clear, strong peaks in the SHG signal scaling with the AlN film thickness (see inset in Fig. 2a with enlarged vertical axis). The observation of such a sizeable SHG yield at the LO frequency is astonishing, especially considering the exceptionally small effective volume of only a few nanometer AlN that is generating the signal.

We argue that the origin of this large SHG yield at the LO frequency, where the second-order susceptibility $\chi^{(2)}$ has no resonances,⁴² is the immense electric field enhancement in the AlN thin film. In order to get further insights into electric field distributions, we employ a 4×4 transfer matrix formalism specifically designed to simultaneously handle media with fully anisotropic as well as isotropic dielectric tensors.⁴⁶ This allows us to account for the uniaxial anisotropy of both 4H-SiC and hexagonal AlN, leading to an accurate reproduction of the reflectance data with highly detailed qualitative accordance. For instance, even small features like the dip at the high-frequency reststrahlen edge of SiC originating from the SiC anisotropy are accurately reproduced, see Fig. 2d. (Note that for Fig. 1 the materials were taken to be isotropic, which is sufficient for the qualitative understanding of the Berreman mode.)

Quantitatively, the calculations feature a deeper and sharper Berreman dip in the reflectance than in the experiments, see Fig. 2b. This discrepancy is mainly due to growth defects in the AlN layer and an unavoidable strain due to the lattice mismatch between SiC and AlN (1%),^{47,48} leading to an effectively increased damping constant of AlN than assumed in the calculations ($\gamma_{AlN} = 2.2 \text{ cm}^{-1}$).⁴⁹ Furthermore, an additional experimental broadening arises from the FEL linewidth ($\sim 4 \text{ cm}^{-1}$).

In Fig. 2c, we show the in-plane (E_x) and out-of-plane (E_z) local electric field enhancements at the AlN/SiC interface in both media. Note that E_x and E_z are normalized to

their respective incoming field amplitudes E_{x0} and E_{z0} . While E_x is conserved at the interface and is generally small (with a maximum value of ~ 1.9), the E_z field enhancement features a very large peak at ω_{LO}^{AlN} with a maximum of ~ 180 for the 10 nm film.

Note that while the Berreman reflectance minimum deepens for larger film thicknesses, the E_z field enhancement is already 16% smaller in the 20 nm than in the 10 nm film. Thus, counter-intuitively, thicker films that feature higher optical absorption, exhibit a smaller degree of field enhancement. In the observed SHG signal, this reduction is compensated by an increasing effective volume, leading to larger SHG yields. However, we emphasize that only ultrathin films ($d_{AlN} < 50 \text{ nm}$) demonstrate such high field intensities, thus opening new possibilities for deeply subwavelength nanophotonic applications in the IR.

The E_z field is fully confined inside the AlN layer, which is reflected in the flat frequency dependence and small magnitude of the E_z field enhancement in SiC (blue line in Fig. 2c). This field localization is even better illustrated in Fig. 3a, where we show the spatial distribution of the in-plane E_x and out-of-plane E_z field enhancements as a function of z , i.e. along the surface normal, at $\omega = 900 \text{ cm}^{-1}$. The electric field has to obey Maxwell's boundary conditions, i.e. continuity of the in-plane fields ($E_x^{SiC} = E_x^{AlN}$ and $E_y^{SiC} = E_y^{AlN}$) and of the out-of-plane displacement field $D_z = \varepsilon E_z$ is required:

$$\varepsilon_{SiC} E_z^{SiC} = \varepsilon_{AlN} E_z^{AlN}. \quad (2)$$

Eq. 2 is the physical reason for the strong field enhancement and field confinement in thin films at ENZ conditions, since for vanishing ε_{AlN} adjacent to SiC with a finite ε_{SiC} , the electric field E_z^{AlN} strongly increases in order to fulfill the boundary condition. We note that on atomistic length scales, however, the dielectric function does not jump abruptly, as suggested by Maxwell's boundary condition, but features a continuous transition.⁵⁰

Fig. 3b and c show spatio-spectral maps of the E_x and E_z fields each normalized to E_{x0}

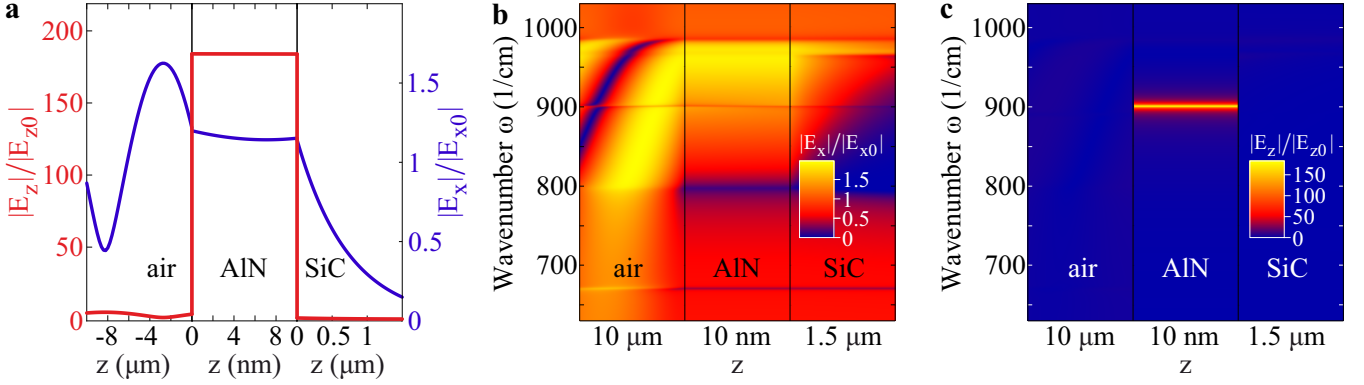


Figure 3: **Field enhancement in a 10 nm thin AlN film.** **a** shows the in-plane and out-of-plane normalized fields E_x and E_z , respectively, along the z axis perpendicular to the interfaces and calculated at the Berreman resonance at 900 cm^{-1} . The tremendous E_z field enhancement (red) is strongly localized inside the AlN. The E_x field (blue), on the other hand, does not feature any significant field enhancement. Note that in the air layer, the sum of the normalized incoming wave and the reflected wave is plotted, thus resulting in amplitudes larger than 1. **b, c** Spatio-spectral maps of E_x and E_z , respectively. The in-plane field E_x features a small enhancement at the SiC LO (965 cm^{-1}) and a minimum at the SiC TO (797 cm^{-1}). In between in the SiC reststrahlen band, the field decays evanescently into the SiC substrate. Interestingly, a local minimum in E_x can be observed at both the AlN TO (670 cm^{-1}) and the AlN LO (900 cm^{-1}). On the contrary, the out-of-plane field E_z in **c** features an immense and spectrally sharp field enhancement inside the AlN layer at the AlN LO frequency.

and E_{z0} , respectively. Interestingly, E_x features no considerable field enhancement, but exhibits small dips or peaks marking the TO and LO frequencies of both AlN and SiC. The spatio-spectral map of E_z in Fig. 3c, on the other hand, clearly reveals the extreme, spectrally sharp and strongly confined field enhancement in the AlN layer at $\omega = 900\text{ cm}^{-1}$.

Finally, we turn to the TO frequency of AlN (670 cm^{-1}),⁵¹ where the experimental data in Fig. 2a exhibit a strong SHG signal of similar magnitude as at the LO frequency. Quite surprisingly, this AlN TO peak is even larger than the peak at the TO frequency of the SiC substrate. Partially, this can be attributed to a reduced field suppression at ω_{TO} for thin films compared to a bulk crystal.⁴⁵ Notably, the observed peak arises from a resonance in the second-order susceptibility $\chi^{(2)}$ at ω_{TO}^{AlN} , and not from a field enhancement as for the LO peak. Therefore, to fully understand the SHG peak amplitudes at the TO frequencies, a quantitative model of the $\chi^{(2)}$ for AlN would be necessary.

In this work, we have observed an immense

SHG signal arising from a Berreman mode in an ultrathin AlN film excited at ENZ frequencies in the mid-IR. Analogous to previous studies of ITO,⁵² aluminum-doped ZnO,⁵³ and CdO,⁵⁴ the high optical nonlinearity at ENZ conditions in our system holds high promises for all-optical ultrafast control of polarization switching,⁵⁴ and even over the material's optical properties.^{52,53} However, while all mentioned studies employ ultrathin films excited via free-space radiation – for which in our system the Berreman mode is accessible, dispersing inside the light cone in vacuum – a complementary polaritonic ENZ mode exists on the other side of the light line. The linear response of these ENZ polaritons has been studied recently,^{55,56} but investigations of their nonlinear response are to the best of our knowledge still lacking. Analogous to the Berreman mode, a tremendous field enhancement also characterizes the ENZ thin film polariton due to its ENZ environment. We therefore highlight the nonlinear response of ENZ polaritons to be an intriguing subject, specifically in light of the development of polariton-based nonlinear nanophotonics.

Polar crystals such as AlN or SiC, where ENZ conditions are met at the LO phonon resonances in the mid-IR, feature several appealing properties that are unavailable in metals or ITO: (i) The imaginary part of the dielectric function ε_2 at ω_{LO} ($\varepsilon_{AlN}(\omega = \omega_{LO}) = 0 + 0.02i$) is significantly smaller than in metals,⁵⁷ and more than one order of magnitude smaller than for ITO ($\varepsilon_{ITO}(\omega = \omega_{LO}) = 0 + 0.5i$),⁴⁰ which strongly increases the field enhancement inside the thin layer and hence the SHG efficiency. (ii) Many polytypes of SiC as well as AlN exhibit a hexagonal crystal structure, resulting in a uniaxial anisotropy of the dielectric tensor. This anisotropy leads to a hyperbolic frequency region between the extraordinary and ordinary LO frequencies, i.e. in the range of the ENZ polaritons, enabling a whole new range of phenomena yet to be explored. These phenomena include, as has been observed in different systems before, negative refraction,⁵⁸ negative phase velocity,⁵⁹ or subdiffraction imaging and focusing.^{60,61} (iii) Due to relatively short lifetimes of surface plasmon polaritons in metals or most highly doped semiconductors, plasmon-based nanophotonics exhibits intrinsic drawbacks due to inherently high losses, whereas SPhPs in polar crystals feature much longer polariton lifetimes due to long-lived phonon resonances.^{8,62} Hence, the employment of the ENZ polariton at the LO frequency offers an appealing alternative for nanophotonic applications, where low-loss ENZ characteristics combine with ultra-high field enhancements.

In conclusion, we have reported the first observation of a resonantly enhanced SHG yield from a phononic Berreman mode in a deeply subwavelength thin film, exemplified for AlN on a 4H-SiC substrate. The origin of this large SHG signal is the immense out-of-plane field enhancement arising due to the zero-crossing of the dielectric function at the thin film LO frequency, strongly confined to the ultrathin layer. Thanks to low phonon dampings in polar crystals such as AlN and SiC, nanophotonic systems based on such crystals offer an appealing alternative to plasmonics, featuring high-quality resonances with extreme field enhancements. As a possible pathway, we envision ultrathin-film

Berreman modes featuring ENZ nature to provide new opportunities for ultrafast all-optical control by taking advantage of the high optical nonlinearity.

Acknowledgement We thank Wieland Schöllkopf and Sandy Gewinner for operating the FEL. D.S.K. and D.F.S. acknowledge funding support from the Office of Naval Research. J.D.C. acknowledges financial support from the Office of Naval Research under grant N00014-18-2107 and from Vanderbilt School of Engineering. We thank Christopher J. Winta for careful reading of the paper.

References

- (1) Kauranen, M.; Zayats, A. V. *Nature Photonics* **2012**, *6*, 737–748.
- (2) Lu, H.; Liu, X.; Wang, L.; Gong, Y.; Mao, D. *Optics Express* **2011**, *19*, 2910.
- (3) Ren, M.; Jia, B.; Ou, J.-Y.; Plum, E.; Zhang, J.; MacDonald, K. F.; Nikolaenko, A. E.; Xu, J.; Gu, M.; Zheludev, N. I. *Advanced Materials* **2011**, *23*, 5540–5544.
- (4) Sederberg, S.; Elezzabi, A. Y. *Physical Review Letters* **2015**, *114*, 227401.
- (5) Shibanuma, T.; Grinblat, G.; Albella, P.; Maier, S. A. *Nano Letters* **2017**, *17*, 2647–2651.
- (6) Nie, S. *Science* **1997**, *275*, 1102–1106.
- (7) Kneipp, K.; Wang, Y.; Kneipp, H.; Perelman, L. T.; Itzkan, I.; Dasari, R. R.; Feld, M. S. *Physical Review Letters* **1997**, *78*, 1667–1670.
- (8) Caldwell, J. D.; Lindsay, L.; Gianini, V.; Vurgaftman, I.; Reinecke, T. L.; Maier, S. A.; Glembocki, O. J. *Nanophotonics* **2015**, *4*, 44–68.
- (9) Hillenbrand, R.; Taubner, T.; Keilmann, F. *Nature* **2002**, *418*, 159–162.

- (10) Wang, T.; Li, P.; Hauer, B.; Chigrin, D. N.; Taubner, T. *Nano Letters* **2013**, *13*, 5051–5055.
- (11) Caldwell, J. D.; Glembocki, O. J.; Francescato, Y.; Sharac, N.; Giannini, V.; Bezares, F. J.; Long, J. P.; Owrutsky, J. C.; Vurgaftman, I.; Tischler, J. G. et al. *Nano Letters* **2013**, *13*, 3690–3697.
- (12) Autore, M.; Li, P.; Dolado, I.; Alfaro-Mozaz, F. J.; Esteban, R.; Atxabal, A.; Casanova, F.; Hueso, L. E.; Alonso-González, P.; Aizpurua, J. et al. *Light: Science & Applications* **2018**, *7*, 17172.
- (13) Chen, Y.; Francescato, Y.; Caldwell, J. D.; Giannini, V.; Maß, T. W. W.; Glembocki, O. J.; Bezares, F. J.; Taubner, T.; Kasica, R.; Hong, M. et al. *ACS Photonics* **2014**, *1*, 718–724.
- (14) Caldwell, J. D.; Kretinin, A. V.; Chen, Y.; Giannini, V.; Fogler, M. M.; Francescato, Y.; Ellis, C. T.; Tischler, J. G.; Woods, C. R.; Giles, A. J. et al. *Nature Communications* **2014**, *5*, 5221.
- (15) Giles, A. J.; Dai, S.; Vurgaftman, I.; Hoffman, T.; Liu, S.; Lindsay, L.; Ellis, C. T.; Assefa, N.; Chatzakis, I.; Reinecke, T. L. et al. *Nature Materials* **2017**, *17*, 134–139.
- (16) Ferrell, R. A. *Physical Review* **1958**, *111*, 1214–1222.
- (17) Berreman, D. W. *Physical Review* **1963**, *130*, 2193–2198.
- (18) McAlister, A. J.; Stern, E. A. *Physical Review* **1963**, *132*, 1599–1602.
- (19) Bösenberg, J.; Raether, H. *Physical Review Letters* **1967**, *18*, 397–398.
- (20) Burke, J. J.; Stegeman, G. I.; Tamir, T. *Physical Review B* **1986**, *33*, 5186–5201.
- (21) Bichri, A.; Lafait, J.; Welsch, H. *Journal of Physics: Condensed Matter* **1993**, *5*, 7361–7374.
- (22) Vassant, S.; Hugonin, J.-P.; Marquier, F.; Greffet, J.-J. *Optics Express* **2012**, *20*, 23971.
- (23) Nordin, L.; Dominguez, O.; Roberts, C. M.; Streyer, W.; Feng, K.; Fang, Z.; Podolskiy, V. A.; Hoffman, A. J.; Wasserman, D. *Applied Physics Letters* **2017**, *111*, 091105.
- (24) Campione, S.; Brener, I.; Marquier, F. *Physical Review B* **2015**, *91*, 121408.
- (25) Li, Y.; Kita, S.; Muñoz, P.; Reshef, O.; Vulis, D. I.; Yin, M.; Lončar, M.; Mazur, E. *Nature Photonics* **2015**, *9*, 738–742.
- (26) Liberal, I.; Engheta, N. *Nature Photonics* **2017**, *11*, 149–158.
- (27) Joannopoulos, J. D.; Johnson, S. G.; Winn, J. N.; Meade, R. D. *Photonic Crystals: Molding the Flow of Light*; Princeton University Press, 2008.
- (28) Burgos, S. P.; de Waele, R.; Polman, A.; Atwater, H. A. *Nature Materials* **2010**, *9*, 407–412.
- (29) Sakoda, K. *Optical Properties of Photonic Crystals*; Springer Series in Optical Sciences; Springer-Verlag: Berlin/Heidelberg, 2005; Vol. 80; p 258.
- (30) Vassant, S.; Archambault, A.; Marquier, F.; Pardo, F.; Gennser, U.; Cavanna, A.; Pelouard, J. L.; Grefet, J. J. *Physical Review Letters* **2012**, *109*, 237401.
- (31) Vassant, S.; Moldovan Doyen, I.; Marquier, F.; Pardo, F.; Gennser, U.; Cavanna, A.; Pelouard, J. L.; Grefet, J. J. *Applied Physics Letters* **2013**, *102*, 081125.
- (32) Vasudev, A. P.; Kang, J.-H.; Park, J.; Liu, X.; Brongersma, M. L. *Optics Express* **2013**, *21*, 26387.

- (33) Luk, T. S.; Campione, S.; Kim, I.; Feng, S.; Jun, Y. C.; Liu, S.; Wright, J. B.; Brener, I.; Catrysse, P. B.; Fan, S. et al. *Physical Review B* **2014**, *90*, 085411.
- (34) Feng, S.; Halterman, K. *Physical Review B* **2012**, *86*, 165103.
- (35) Berini, P. *Physical Review B* **2001**, *63*, 125417.
- (36) Berini, P. *Advances in Optics and Photonics* **2009**, *1*, 484.
- (37) Vincenti, M. A.; de Ceglia, D.; Ciattoni, A.; Scalora, M. *Physical Review A* **2011**, *84*, 063826.
- (38) Capretti, A.; Wang, Y.; Engheta, N.; Dal Negro, L. *ACS Photonics* **2015**, *2*, 1584–1591.
- (39) Luk, T. S.; de Ceglia, D.; Liu, S.; Keeler, G. A.; Prasankumar, R. P.; Vincenti, M. A.; Scalora, M.; Sinclair, M. B.; Campione, S. *Applied Physics Letters* **2015**, *106*, 151103.
- (40) Capretti, A.; Wang, Y.; Engheta, N.; Dal Negro, L. *Optics Letters* **2015**, *40*, 1500.
- (41) Raether, H. *Surface Plasmons on Smooth and Rough Surfaces and on Gratings*; Springer Tracts in Modern Physics; Springer Berlin Heidelberg: Berlin, Heidelberg, 1988; Vol. 111.
- (42) Paarmann, A.; Razdolski, I.; Melnikov, A.; Gewinner, S.; Schöllkopf, W.; Wolf, M. *Applied Physics Letters* **2015**, *107*, 081101.
- (43) Schöllkopf, W.; Gewinner, S.; Junkes, H.; Paarmann, A.; von Helden, G.; Bluem, H.; Todd, A. M. M. The new IR and THz FEL facility at the Fritz Haber Institute in Berlin. 2015; p 95121L.
- (44) Passler, N. C.; Razdolski, I.; Gewinner, S.; Schöllkopf, W.; Wolf, M.; Paarmann, A. *ACS Photonics* **2017**, *4*, 1048–1053.
- (45) Paarmann, A.; Razdolski, I.; Gewinner, S.; Schöllkopf, W.; Wolf, M. *Physical Review B* **2016**, *94*, 134312.
- (46) Passler, N. C.; Paarmann, A. *Journal of the Optical Society of America B* **2017**, *34*, 2128.
- (47) Tairov, Y.; Tsvetkov, V. *Progress in Crystal Growth and Characterization* **1983**, *7*, 111–162.
- (48) Taylor, K. M.; Lenie, C. *Journal of The Electrochemical Society* **1960**, *107*, 308.
- (49) Moore, W. J.; Freitas, J. A.; Holm, R. T.; Kovalenkov, O.; Dmitriev, V. *Applied Physics Letters* **2005**, *86*, 141912.
- (50) Zheng, D.-S.; Wang, Y.; Liu, A.-A.; Wang, H.-F. *International Reviews in Physical Chemistry* **2008**, *27*, 629–664.
- (51) Davydov, V. Y.; Kitaev, Y. E.; Goncharuk, I. N.; Smirnov, A. N.; Graul, J.; Semchinova, O.; Uffmann, D.; Smirnov, M. B.; Mirgorodsky, A. P.; Evarestov, R. A. *Physical Review B* **1998**, *58*, 12899–12907.
- (52) Alam, M. Z.; De Leon, I.; Boyd, R. W. *Science* **2016**, *352*, 795–797.
- (53) Kinsey, N.; DeVault, C.; Kim, J.; Ferrera, M.; Shalae, V. M.; Boltasseva, A. *Optica* **2015**, *2*, 616.
- (54) Yang, Y.; Kelley, K.; Sachet, E.; Campione, S.; Luk, T. S.; Maria, J.-P.; Sinclair, M. B.; Brener, I. *Nature Photonics* **2017**, *11*, 390–395.
- (55) Passler, N. C.; Gubbin, C. R.; Folland, T. G.; Razdolski, I.; Katzer, D. S.; Storm, D. F.; Wolf, M.; De Liberato, S.; Caldwell, J. D.; Paarmann, A. *Nano Letters* **2018**, *18*, 4285–4292.
- (56) Runnerstrom, E. L.; Kelley, K. P.; Folland, T. G.; Engheta, N.; Caldwell, J. D.; Maria, J.-P. *ArXiv e-prints* **2018**,

- (57) LYNCH, D. W.; HUNTER, W. *Handbook of Optical Constants of Solids*; Elsevier, 1985; Vol. 1; pp 275–367.
- (58) Rodrigues da Silva, R.; Macêdo da Silva, R.; Dumelow, T.; da Costa, J. A. P.; Honorato, S. B.; Ayala, A. P. *Physical Review Letters* **2010**, *105*, 163903.
- (59) Yoxall, E.; Schnell, M.; Nikitin, A. Y.; Txoperena, O.; Woessner, A.; Lundeborg, M. B.; Casanova, F.; Hueso, L. E.; Koppens, F. H. L.; Hillenbrand, R. *Nature Photonics* **2015**, *9*, 674–678.
- (60) Li, P.; Lewin, M.; Kretinin, A. V.; Caldwell, J. D.; Novoselov, K. S.; Taniguchi, T.; Watanabe, K.; Gaussmann, F.; Taubner, T. *Nature Communications* **2015**, *6*, 7507.
- (61) Dai, S.; Ma, Q.; Andersen, T.; Mcleod, A. S.; Fei, Z.; Liu, M. K.; Wagner, M.; Watanabe, K.; Taniguchi, T.; Thiemens, M. et al. *Nature Communications* **2015**, *6*, 6963.
- (62) Khurgin, J. B. *Nature Nanotechnology* **2015**, *10*, 2–6.